

Growth of entanglement of generic states under dual-unitary dynamics

Alessandro Foligno^{1,2} and Bruno Bertini^{1,2}

¹*School of Physics and Astronomy, University of Nottingham, Nottingham, NG7 2RD, UK*

²*Centre for the Mathematics and Theoretical Physics of Quantum Non-Equilibrium Systems, University of Nottingham, Nottingham, NG7 2RD, UK*

Dual-unitary circuits are a class of locally-interacting quantum many-body systems displaying unitary dynamics also when the roles of space and time are exchanged. These systems have recently emerged as a remarkable framework where certain features of many-body quantum chaos can be studied exactly. In particular, they admit a class of “solvable” initial states for which, in the thermodynamic limit, one can access the full non-equilibrium dynamics. This reveals a surprising property: when a dual-unitary circuit is prepared in a solvable state the quantum entanglement between two complementary spatial regions grows at the *maximal* speed allowed by the local structure of the evolution. Here we investigate the fate of this property when the system is prepared in a *generic* pair-product state. We show that in this case the entanglement increment during a time step is sub-maximal for finite times, however, it approaches the maximal value in the infinite-time limit. This statement is proven rigorously for dual-unitary circuits generating high enough entanglement, while it is argued to hold for the entire class.

I. INTRODUCTION

The evolution of quantum entanglement gives a universal and unifying characterisation of non-equilibrium dynamics in a wide range of quantum many-body systems ranging from lattice models to relativistic field theories [1–4]. Whereas the analysis of specific local observables is clouded by a plethora of system- and observable-specific effects, the evolution of entanglement over large scales does not depend on such inessential details and returns a fair portrait of the full (generalised) thermalisation process [5, 6]. Whenever a quantum many-body system with local interactions is prepared in an out-of-equilibrium state with low entanglement, and then let to follow its own unitary evolution, the entanglement between different spatial regions is observed to grow in time, signalling the proliferation of quantum correlations. In the course of this process the entanglement entropy of a given subsystem is transformed into *thermodynamic entropy* and eventually saturates to a time-independent value indicating the onset of relaxation [5, 7–10]. Unless specific competing mechanisms are introduced — such as disorder [11–13], confinement [14], or local measurements [15–17] — the entanglement grows linearly in time, irrespective of the nature of the system dynamics [5, 6, 10, 18–33].

The linear growth of entanglement naturally defines a velocity — known as *entanglement velocity* [6, 23, 31] — which is obtained dividing the slope of the growth by the density of stationary entropy. The entanglement velocity is the key emergent parameter of the thermalisation process: it gives information on when subsystems start approaching stationarity and, at the same time, determines the feasibility of classical simulations of the quantum dynamics [34–37]. While it is clear that the entanglement velocity depends on geometry and couplings of a given system [10, 28, 38], it is less obvious whether it also depends on the initial configuration. One might expect that for systems producing enough scrambling of quan-

tum information the dependence on the initial configuration should be mild, and all configurations leading to the same stationary state are characterised by the same entanglement velocity. On the other hand, the entanglement velocity describes a truly out-of-equilibrium regime taking place prior to relaxation and when a full scrambling of quantum information has yet to take place. For free systems for instance, where each conserved mode decoheres to a stationary state and has a different entanglement velocity [5], one can show that initial configurations leading to the same stationary state can have different sets of entanglement velocities [19]. The same is expected for interacting integrable systems, where a formula for the entanglement velocity of conserved modes [10, 38] is only known for a special class of initial states [39, 40]. For quantum chaotic systems, however, the question is still open.

Here we analyse this question in the context of chaotic “local quantum circuits”, i.e., chains of qudits evolved by discrete applications of local unitary operators. These systems are useful idealisations of generic quantum matter and, over the last few years, have helped understanding information spreading [6, 25, 28, 31, 41–44], spectral statistics [45–55], and thermalisation [26, 32, 51, 56] in quantum many-body systems. Specifically, here we consider a particular class of local quantum circuits known as “dual unitary circuits” [57], which are defined by the property that their bulk dynamics remain unitary also when exchanging the roles of space and time. The most remarkable feature of these systems is that, despite being quantum chaotic, they allow for exact calculations of many relevant many-body quantities [27, 50, 58–69]. Surprisingly, even the very quantum chaotic nature of dual-unitary circuits can be rigorously proven [45, 49].

Dual-unitary circuits admit a class of “solvable” initial states [25, 26], whose dynamics can be characterised exactly in the thermodynamic limit [25, 26, 65, 70]. When evolving from solvable states dual-unitary circuits display *maximal* entanglement growth, namely they show

the largest entanglement growth compatible with the local structure of the time-evolution [25, 26]. In fact, it has been recently shown in Ref. [71] that such a maximal growth is only attainable in dual-unitary circuits. For generic initial states, however, dual-unitarity does not provide any obvious simplification and exact calculations fall out of reach. In addition, many of the special features of the dynamics of solvable states, including the maximal growth of entanglement, are observed to disappear in finite-time numerical experiments [25, 26, 65].

Here we show that, surprisingly, some exact statements can be made also in for generic initial states. In particular, we consider the entanglement evolution from “generic pair-product states”, i.e., non-solvable states written as products of arbitrary two-site states, and show that the entanglement velocity is *maximal* for *almost all* dual-unitary circuits. Therefore, it is *almost always* independent of the initial configuration.

To find these results, we introduce spacetime-dependent noise that preserves dual-unitarity and show that the entanglement velocity averaged over the noise approaches the maximal value for large times. We then prove that this implies asymptotic maximality of the entanglement velocity for each realisation. Our statements are established rigorously for circuits made of dual-unitary gates with high enough “entangling power”, which measures how much a gate can entangle two qubits. These include dual-unitary gates constructed with complex Hadamard matrices [72] and four-leg perfect tensors [73, 74]. We also we present a constructive way — supported by numerical checks — to extend them.

The rest of this paper is laid out as follows. In Sec. II we introduce the systems and initial states considered in this work. In Sec. III we introduce the entanglement velocity, which is the observable of interest, and review its calculation for dual-unitary circuits evolving from solvable states. Sec. IV contains our main results: we begin by introducing the space-time dependent noise and show how maximality on average implies maximality for each single realisation. In Sec. IV A we bound from below the averaged entanglement entropy with a function depending on the gates solely through their entangling power. Then, in Sec. IV B, we prove maximality on average for circuits made of gates with large enough entangling power, while in Sec. IV C we argue that the proof can be extended to all dual-unitary circuits. Finally in Sec. IV D we present some supporting numerical evidence. Our conclusions and final remarks are reported in Sec. V. The four appendices contain a number of complementary technical points.

II. SETTING

A one-dimensional local quantum circuit is a chain of $2L$ qudits — with d internal states — where the evolution occurs in discrete time-steps and describes local interactions. In particular, considering circuits where the

time evolution is implemented in the so called “brickwork” geometry, we write the unitary operator evolving the system from time t to time $t + 1$ as

$$\mathbb{U}(t) = \mathbb{U}_2(t) \cdot \mathbb{U}_1(t), \quad (1)$$

where we introduced

$$\mathbb{U}_1(t) = \bigotimes_{x \in \mathbb{Z}_L} U_{x,t}, \quad \mathbb{U}_2(t) = \bigotimes_{x \in \mathbb{Z}_L + \frac{1}{2}} U_{x,t+1/2}. \quad (2)$$

The operator $U_{x,t}$ acts non-trivially, as the $d^2 \times d^2$ unitary matrix $U(x,t)$, only on the qudits at positions x and $x+1/2$. The matrices $\{U(x,t)\}$ are known as “local gates” and encode the physical properties of the system. In particular, whenever

$$U(x,t) = U, \quad \forall x,t, \quad (3)$$

the evolution operator is invariant under two-site shifts in time and space. We will refer to this case as a spacetime translational invariant quantum circuit.

Note that in Eq. (2) we labelled sites by half integers and assumed periodic boundary conditions so that the (half-odd) integers x and $x + L$ denote the same site. We also remark that the form (1) of the time-evolution operator implies that there is a strict maximal speed for the propagation of correlations. This means that any pair of local operators a_x and b_y evolved up to time t satisfy

$$[a_x(t), b_y(t)] = 0, \quad \lceil |x| - |y| \rceil > 2v_{\max}t, \quad (4)$$

where $\lceil \bullet \rceil$ denotes the ceiling function (smallest integer larger or equal to the argument). Moreover, our choice of units implies a maximal speed $v_{\max} = 1$.

We consider a particular class of local quantum circuits called dual-unitary circuits [57]. Their defining property is that they are generated by local gates that remain unitary under a particular reshuffling which corresponds to switching space and time. More precisely, defining a matrix \tilde{U} with elements

$$\tilde{U}_{(j,l);(i,k)} = U_{(i,j);(k,l)}, \quad i, j, k, l = 0, \dots, d-1, \quad (5)$$

where we set $(i, j) = i * d + j$, we require

$$U^\dagger U = U U^\dagger = I, \quad \tilde{U}^\dagger \tilde{U} = \tilde{U} \tilde{U}^\dagger = I. \quad (6)$$

Whilst the first condition is the standard unitarity requirement for the local gate, the second one is imposing that the gate acts as a unitary matrix also when the roles of space and time are swapped. These constraints admit solution for all local Hilbert space dimensions $d \geq 2$, however, a full parameterisation is only known for $d = 2$ [49, 57, 62, 72, 75, 76]. It is also useful to recall that, even though some of the solutions to (6) are integrable [59, 62, 76, 77], i.e., generate evolution operators with an extensive number of local conserved charges, the integrable instances can only form a lower dimensional sub-manifold of the total manifold of dual-unitary circuits. This can be intuitively understood by

noting that the two equations (6) are left invariant by the transformation

$$U \mapsto u_+ \otimes u_- \cdot U \cdot v_+ \otimes v_-, \quad (7)$$

with u_+, \dots, v_- arbitrary elements of the group of $d \times d$ unitary matrices, which we denote by $U(d)$. This transformation is generally enough to break any non-trivial conservation law. In other words, dual unitary circuits are *generally* non-integrable or quantum chaotic.

A. Entangling Power

A feature of the local gate U which will prove to be important in the following is its *entangling power*. The latter is a measure of the average entanglement produced by U when acting on Haar-random product states, see, e.g., Ref. [78]. In particular, as shown in Refs. [78–80], for dual-unitary circuits it can be expressed as

$$p = \frac{d^4 - \text{tr}[(\tilde{U}^{t_2}(\tilde{U}^{t_2})^\dagger)^2]}{d^2(d^2 - 1)}, \quad (8)$$

where $(\cdot)^{t_2}$ denotes the partial transpose with respect to the second qudit. From (8) one can immediately verify that p is invariant under (7).

As we recall in Appendix A, the entangling power (8) fulfils

$$0 \leq p \leq 1. \quad (9)$$

The lower bound is attained when $\tilde{U}^{t_2}(\tilde{U}^{t_2})^\dagger/d^2$ is a rank-1 projector. This happens when, up to the transformation (7), U coincides with the SWAP gate. Namely, it merely swaps the states of the two qudits it acts on, generating no entanglement. Instead, the upper bound is attained for

$$\tilde{U}^{t_2}(\tilde{U}^{t_2})^\dagger = (\tilde{U}^{t_2})^\dagger \tilde{U}^{t_2} = I. \quad (10)$$

To understand this condition it is useful to think of U a state of four qudits with amplitudes $\{U_{(a_1, a_2); (a_3, a_4)}\}$. In this language, Eq. (10) means that the subset formed by the first and fourth qudits is maximally entangled with its complement. Recalling that the gate U also fulfils (6) we see that also the subsets formed by first and second and first and third qudits are maximally entangled with their complements. In fact, in the state defined by U any bipartition of the four qudits has maximal entanglement with its complement. Gates generating states with this property are called *perfect tensors* [81–83]. Perfect tensors with four entries exist for every local Hilbert space dimension strictly larger than $d = 2$ [73, 74] and, therefore, for $d > 2$ the upper bound $p = 1$ can be attained. Instead, for $d = 2$ the maximal value that p can attain is [57]

$$p = \frac{d}{d+1}, \quad (11)$$

and, up to (7), it is attained by local gates of the form

$$U_{(ab), (cd)} = \delta_{ad} \delta_{bc} \exp\left(i \frac{2\pi ab}{d}\right). \quad (12)$$

The family (12) of dual-unitary gates has been constructed in Ref. [72] using complex Hadamard matrices. Here, for brevity, we call it the ‘‘Hadamard family’’.

B. Quantum Quench

To study the out-of-equilibrium dynamics of the circuits we consider a standard quantum quench protocol: we prepare them a non-equilibrium state $|\Psi_0\rangle$ and let them evolve according to their time-evolution operator. In particular, we consider generic ‘‘pair-product’’ states of the form

$$|\Psi_0\rangle = \frac{1}{d^{L/2}} \bigotimes_{x=1}^L \left(\sum_{i,j=0}^{d-1} m_{i;j} |i, j\rangle \right), \quad (13)$$

where $\{|i\rangle\}_{i=0}^d$ is a basis of the local Hilbert space and matrix m , with elements $m_{i;j}$, fulfils

$$\text{tr}(mm^\dagger) = d, \quad (14)$$

which ensures that $|\Psi_0\rangle$ is normalised to one. Apart from this condition, the matrix m is *completely generic*.

The evolution quantum circuits can be conveniently represented graphically. One depicts the local gates as a four leg tensors

$$U_{(i,j);(k,l)} = \begin{array}{c} k \quad l \\ \diagdown \quad \diagup \\ \square \\ \diagup \quad \diagdown \\ i \quad j \end{array}, \quad (15)$$

and the initial state matrix m as a two-leg one

$$m_{i;j} = \begin{array}{c} i \quad j \\ \diagdown \quad \diagup \\ \bullet \end{array}. \quad (16)$$

When it does not lead to confusion the indices can be dropped to represent the actual tensor instead of its elements. For instance, (6) are conveniently represented as

$$\begin{array}{c} \diagdown \quad \diagup \\ \square \\ \diagup \quad \diagdown \end{array} = \begin{array}{c} \diagdown \quad \diagup \\ \square \\ \diagup \quad \diagdown \end{array} = \begin{array}{c} | \\ | \end{array}, \quad (17)$$

$$\begin{array}{c} \diagdown \quad \diagup \\ \square \\ \diagup \quad \diagdown \end{array} = \begin{array}{c} \diagdown \quad \diagup \\ \square \\ \diagup \quad \diagdown \end{array} = \begin{array}{c} \text{---} \\ \text{---} \end{array}, \quad (18)$$

where we introduced the diagram

$$U^\dagger = \begin{array}{c} \diagup \quad \diagdown \\ \square \text{ (blue)} \\ \diagdown \quad \diagup \end{array} . \quad (19)$$

Instead, the state at time t is depicted as

$$\mathbb{U}^t |\Psi_0\rangle = \begin{array}{c} \text{Diagram of a brickwork lattice with red squares and dashed lines} \\ \text{Equation (20)} \end{array} \quad (20)$$

where we took $L = 4$ and $t = 2$, we represented the matrix multiplication from bottom to top and we conveniently depicted the space-time translational invariant case with periodic boundary conditions. The representation in Eq. (20) makes it clear why this particular way of applying local gates is called brickwork geometry.

III. ENTANGLEMENT GROWTH

In this paper we are interested in the evolution of the entanglement between a contiguous block of $2L_A$ qudits, $A = \{x_1, x_1 + 1/2, \dots, x_2\}$, and its complement, $\bar{A} = \{1/2, \dots, L\} \setminus A$, in the state (20). In particular, we will focus on the regime where the entanglement typically grows linearly in time [5, 6, 10, 18–33], i.e.,

$$2v_{\max}t \leq L_A \leq L - L_A. \quad (21)$$

Since we are considering systems with local interactions, the entanglement between A and \bar{A} is produced starting from the boundaries between the two sub-systems. In the regime of interest the two boundaries between A and \bar{A} are causally disconnected and give identical contributions.

To quantify the entanglement of the bipartition we compute the reduced density matrix

$$\rho_A(t) = \text{tr}_{\bar{A}}[\mathbb{U}^t |\Psi_0\rangle\langle\Psi_0| \mathbb{U}^{-t}], \quad (22)$$

and evaluate its Rényi entropies

$$S_A^{(\alpha)}(t) = \frac{1}{1-\alpha} \log \text{tr}[\rho_A(t)^\alpha], \quad \alpha \in \mathbb{R}. \quad (23)$$

Note that $S_A^{(\alpha)}(t)$ is non-increasing in α

$$S_A^{(\alpha)}(t) \leq S_A^{(\beta)}(t), \quad \alpha \geq \beta, \quad (24)$$

and its limiting value for $\alpha \rightarrow 1$ corresponds to the celebrated *entanglement entropy*

$$\lim_{\alpha \rightarrow 1} S_A^{(\alpha)}(t) = -\text{tr}[\rho_A(t) \log \rho_A(t)] \equiv S_A(t), \quad (25)$$

which is a bona fide measure of bipartite entanglement [1].

To analyse Rényi entropies in the regime (21) we note that the reduced density matrix can be represented as

$$\rho_A(t) = \frac{1}{d^{2t+L_A}} \begin{array}{c} \text{Diagram of a brickwork lattice with blue and red squares and dashed lines} \\ \text{Equation (26)} \end{array} \quad (26)$$

where we used the two-site product form of the initial state (13), the normalisation (14), the unitarity of the gates U , and we introduced the diagram

$$m^\dagger = \begin{array}{c} \bullet \text{ (blue)} \\ \diagdown \quad \diagup \end{array} . \quad (27)$$

Using the representation (26) and employing the unitarity relations (17) one can readily show that if

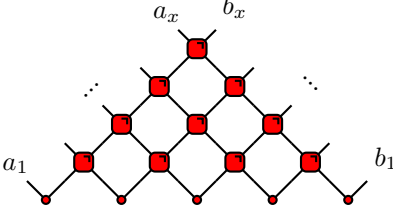
$$2t < |[x_2] - [x_1]|, \quad (28)$$

the traces of powers of the reduced density matrix $\rho_A(t)$

factorise as follows

$$\text{Tr}[\rho_A(t)^\alpha] = \text{Tr}[(C_{2t_{x_2}}^\dagger C_{2t_{x_2}})^\alpha] \text{Tr}[(C_{2t_{x_1}}^\dagger C_{2t_{x_1}})^\alpha]. \quad (29)$$

Here $t_{x_i} = t - \{x_i\}$ ($\{\bullet\} \equiv [\bullet] - \bullet$ is the fractional part) and C_x is a $d^x \times d^x$ matrix corresponding to the following diagram

$$[C_x]_{a;b} = \frac{1}{d^{\frac{x}{2}}}, \quad (30)$$


where q_j denotes the j -th digit of q in base d . Thanks to the unitarity of the local gates, we have the condition

$$\text{Tr}[C_x C_x^\dagger] = 1, \quad \forall x. \quad (31)$$

To simplify the notation, from now on we assume x_1, x_2 to be integers. Plugging (29) into (23), we can express the Rényi entropies as

$$S_A^{(\alpha)}(t) = \frac{2}{1-\alpha} \log \text{Tr}[(C_{2t}^\dagger C_{2t})^\alpha], \quad (32)$$

where the factor of 2 occurs because the two independent boundaries between A and \bar{A} give the same contribution.

Since $C_x C_x^\dagger$ is Hermitian, positive definite, and fulfils (31) it is easy to find a bound for the powers of its trace. To see this, we diagonalise the matrix and express the above conditions in terms of its eigenvalues λ_i as follows

$$\lambda_i \geq 0, \quad \sum_{i=1}^{\mathcal{N}} \lambda_i = 1, \quad (33)$$

where $\mathcal{N} = d^x$ is the dimension of the vector space on which the matrix acts. The constraints (33) on generic real numbers lead to the following bound

$$\frac{1}{\mathcal{N}^{\alpha-1}} \leq \text{Tr}[(C_x^\dagger C_x)^\alpha] = \sum_i \lambda_i^\alpha \leq 1, \quad \forall \alpha \geq 1 \quad (34)$$

Using this in (32), we find

$$0 \leq S_A^{(\alpha)}(t) \leq 4t \log d, \quad \forall \alpha \geq 1. \quad (35)$$

The lower bound is reached when $C_x^\dagger C_x$ is a projector on a one-dimensional space, while the upper bound is attained when it is maximally mixed, i.e.

$$C_x C_x^\dagger = \frac{\mathbb{1}_x}{d^x}, \quad (36)$$

where $\mathbb{1}_x$ is the identity matrix on x qudits.

We are now in a position to introduce the observable of interest in this paper, i.e., the *entanglement velocity*, which quantifies the asymptotic growth of entanglement

in the out-of-equilibrium regime (21). In our setting this quantity is defined as the ratio between half of the asymptotic slope of the entanglement entropy and the density of entropy of the stationary state — the additional factor of two is included to isolate the the entanglement growth from a single boundary between A and \bar{A} . More formally, for a circuit without local conservation laws, we have

$$v_E \equiv \limsup_{t \rightarrow \infty} \lim_{L_A \rightarrow \infty} \lim_{L \rightarrow \infty} \frac{S_A(t)}{4t \log d}. \quad (37)$$

Note that in (37) we used that the circuit has no local conservation laws to find the density of its thermodynamic entropy ($2 \log d$) and we introduced the limit superior rather than the regular limit to make sure that v_E always exists. Analogously, we can introduce entanglement velocities for all Rényi entropies

$$v_{E,\alpha} \equiv \limsup_{t \rightarrow \infty} \lim_{L_A \rightarrow \infty} \lim_{L \rightarrow \infty} \frac{S_A^{(\alpha)}(t)}{4t \log d}, \quad v_{E,1} = v_E. \quad (38)$$

Using (24) and (35) we find the following general bound

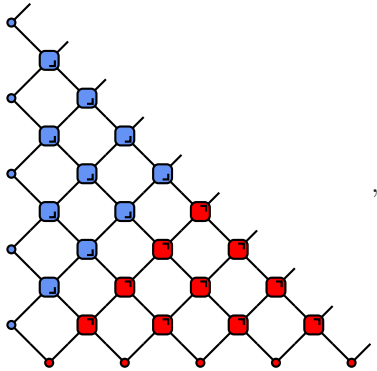
$$0 \leq v_{E,\beta} \leq v_{E,\alpha} \leq 1, \quad \beta \geq \alpha. \quad (39)$$

Note that, up to now, we did not use the dual-unitarity of the gates at any point in the reasoning and, in fact, our discussion applies to any chaotic local quantum circuit. This is because generic matrices m “break” the special dual-unitarity property of the local gates, preventing any direct simplification. On the other hand, as we shall now see, for a special class of compatible matrices, dual-unitarity immediately leads to an explicit expression for $S_A^{(\alpha)}(t)$.

Let us consider a sub-class of pair-product states (13) characterised by *unitary* matrices m , i.e., matrices fulfilling the diagrammatic relations

$$\begin{array}{c} | \\ \bullet \\ \text{---} \\ \bullet \\ | \end{array} = \begin{array}{c} | \\ \bullet \\ \text{---} \\ \bullet \\ | \end{array} = \begin{array}{c} | \\ \text{---} \\ | \end{array}. \quad (40)$$

Repeatedly applying (40) and (18) we can fully contract the tensor network

$$C_x^\dagger C_x = \begin{array}{c} \begin{array}{c} | \\ \bullet \\ \text{---} \\ \bullet \\ | \end{array} \\ \text{---} \\ \begin{array}{c} | \\ \bullet \\ \text{---} \\ \bullet \\ | \end{array} \end{array}, \quad (41)$$


and find

$$C_x^\dagger C_x = \frac{\mathbb{1}_x}{d^x}. \quad (42)$$

Pair-product initial states with this property are part of a larger family of exactly treatable states, generically in MPS form, called *solvable states* [26].

We see that, for solvable pair product states, $C_x^\dagger C_x$ takes the maximally mixed form (36), therefore the entropies saturate the bound (35), i.e.,

$$S_A^{(\alpha)}(t) = 4t \log d, \quad \forall \alpha, \quad (43)$$

or, equivalently, all entropies have the *maximal* increment over a time step

$$\Delta S_A^{(\alpha)}(t) \equiv \frac{S_A^{(\alpha)}(t) - S_A^{(\alpha)}(t-1)}{4 \log d} = 1, \quad \forall \alpha. \quad (44)$$

This condition characterises all solvable states for large enough subsystems [26]. A particular consequence of this is also

$$v_E = 1. \quad (45)$$

The goal of this paper is to show that, even if hidden, an effect of dual-unitarity is also present for generic initial states m . As a consequence, even if (44) does not hold at finite times, the entanglement velocity *remains maximal*.

IV. ENTANGLEMENT VELOCITY FROM GENERIC PAIR-PRODUCT STATES

Our strategy to treat generic initial states is to introduce spacetime-dependent noise and to show that our statements hold for arbitrary distributions of the noise. More specifically, we consider a spacetime translational invariant, dual-unitary circuit characterised by a local gate U , and insert uncorrelated Haar-distributed $U(d)$ noise at each spacetime point through the transformation (7). Note that the family of random dual-unitary gates we produce in this way is a direct generalisation, for generic d , of the family introduced in [84].

In this random setting it is natural to consider the averaged Rényi entropies

$$\bar{S}_A^{(\alpha)}(t) = \frac{1}{1-\alpha} \mathbb{E}[\log \text{tr}(\rho_A(t)^\alpha)], \quad (46)$$

where $\mathbb{E}[\cdot]$ is the average over the set of unitaries

$$\mathbf{u} \equiv \{u_\pm(\tau, x), v_\pm(\tau, x)\}_{\tau=1, \dots, t; x=1, \dots, L} \in U^{4Lt}(d), \quad (47)$$

and $U^x(d)$ denotes the direct product of x copies of $U(d)$.

Analogously, we define the averaged entanglement velocities as

$$\bar{v}_{E,\alpha} \equiv \limsup_{t \rightarrow \infty} \lim_{L \rightarrow \infty} \lim_{L \rightarrow \infty} \frac{\bar{S}_A^{(\alpha)}(t)}{4t \log d}, \quad \bar{v}_E = \bar{v}_{E,1}. \quad (48)$$

With these definitions at hand, we are now in a position to state our main objective. Our goal is to prove the following property.

Property 1. *For all states of the form (13)*

$$\bar{v}_E = 1. \quad (49)$$

Before approaching the proof, let us analyse its implications. Recalling the bound in Eq. (39) we see that this property implies that the average entanglement velocity is maximal for any initial state (13). Since we find our bound saturated on average, we intuitively expect the entanglement velocity to be maximal for almost every choice of the unitaries \mathbf{u} . To make this statement more precise, consider the function f whose superior limit for $t \rightarrow \infty$ is the entanglement velocity

$$f(t, \{u_\pm(t, x)\}, \{v_\pm(t, x)\}) \equiv \lim_{L \rightarrow \infty} \lim_{L \rightarrow \infty} \frac{S_A(t)}{4t \log(d)}. \quad (50)$$

Note that, for any choice of the gates we have

$$f(t, \{u_\pm(t, x)\}, \{v_\pm(t, x)\}) \in [0, 1]. \quad (51)$$

Here we make this function depend on an semi-infinite square grid of gates, labelled by (x, t) , with $t = 1, 2, \dots, \infty$ and $x = -\infty, \dots, \infty$ (at finite times t it actually depends only on a finite subset of such gates). This function is measurable for any t because it is continuous [85]: its associated measure Ω is the product of the Haar measures of each unitary $u_\pm(t, x), v_\pm(t, x)$. Importantly, the measure Ω is fixed and does not depend on t because it is a countable product of Haar measures on the semi-infinite square grid described above. Since f is positive and measurable for any t , we can apply Fatou's lemma [85] and exchange the order between limsup and integral

$$\int d\Omega v_E = \int d\Omega \limsup_{t \rightarrow \infty} f \geq \limsup_{t \rightarrow \infty} \int d\Omega f = \bar{v}_E = 1, \quad (52)$$

where, in the last equality, we used Property 1. Given the bound (51), we immediately find

$$\int d\Omega v_E = 1. \quad (53)$$

Since this saturates the bound on the velocity, it is implied that, for almost all choices of gates, the entanglement velocity is 1, i.e.,

$$\bar{v}_E = 1 \implies v_E \approx 1. \quad (54)$$

Here the symbol \approx indicates that the equality holds for *almost all* choices of gates.

In the upcoming subsections we prove Property 1. In Sec. IV A we show that $\bar{S}_A(t)$ can be bounded from below in terms of a function depending on the gates only through the entangling power of U . In Sec. IV B we show that for

$$p \geq \bar{p}(d) \equiv \frac{d^2 - 1}{d^2} \left(1 - \frac{1}{\sqrt{2d+2}} \right), \quad (55)$$

this bound leads to a rigorous proof of Property 1. In particular, recalling Sec. II A and noting that

$$\bar{p}(d) < \frac{d}{d+1} < 1, \quad (56)$$

we prove that Property 1 holds for perfect tensors and for the Hadamard family. In Subsection IV C, instead, we argue that Property 1 can be extended to all p except for a neighbourhood of $p = 0$. Finally, in Sec. IV D we present numerical evidence supporting the claim that v_E is one for concrete individual realisations of the noise.

A. Bound on $\bar{S}_A(t)$

We aim to bound $\bar{S}_A(t)$ in the regime (21) by a function depending on the local gates only through p . We begin by using (24) and (35) which give

$$\bar{S}_A^{(2)}(t) \leq \bar{S}_A(t) \leq 4t \log d, \quad (57)$$

Noting now that the function

$$f(x) = -2 \log x, \quad (58)$$

is convex, we have

$$-2 \log \mathcal{P}_{2t} \leq \bar{S}_A^{(2)}(t), \quad (59)$$

where we introduced the averaged purity for the matrix $C_x^\dagger C_x$

$$\mathcal{P}_x \equiv \mathbb{E}[\text{Tr}[(C_x^\dagger C_x)^2]]. \quad (60)$$

Putting all together we have

$$-2 \log \mathcal{P}_{2t} \leq \bar{S}_A(t) \leq 4t \log d. \quad (61)$$

To conclude, we show that \mathcal{P}_x depends on the local gates only through their entangling power. To this end, we note that, since \mathbf{u} are independently distributed at each spacetime point, the average $\mathbb{E}[\cdot]$ factorises on each separate gate. This allows us to adopt a convenient tensor-network representation for \mathcal{P}_x , which is obtained by folding the four diagrams for C_x, C_x^\dagger, C_x , and C_x^\dagger on top of each other and averaging (see Ref [84] for a more detailed explanation of this ‘‘folded’’ diagrammatic representation)

$$\mathcal{P}_x = \left\langle \begin{array}{c} \text{Diagram: A diamond-shaped lattice of green squares and white circles connected by lines, representing the folded tensor network for } \mathcal{P}_x. \end{array} \right\rangle, \quad (62)$$

where we introduced the vectors

$$\begin{aligned} |\circ\rangle &\equiv \frac{1}{d} \sum_{i,j,k,l} \delta_{ij} \delta_{kl} |ijkl\rangle, \\ |\square\rangle &\equiv \frac{1}{d} \sum_{i,j,k,l} \delta_{il} \delta_{jk} |ijkl\rangle, \end{aligned} \quad (63)$$

and the averaged gate

$$W = \left\langle \begin{array}{c} \text{Diagram: A green square with four lines extending from its corners, representing the averaged gate } W. \end{array} \right\rangle = (P \otimes P)(U \otimes_r U^*)^{\otimes r^2} (P \otimes P). \quad (64)$$

Here \otimes_r denotes the tensor product over replicas rather than spatial sites, and the operator

$$P = \mathbb{E}[(v \otimes_r v^*)^{\otimes r^2}] \quad v \in U(d), \quad (65)$$

is a projector on a 2-dimensional space spanned by the vectors (63) (see, e.g., Appendix G of Ref. [41] for an elementary proof). Note that these states are linearly independent but not orthogonal, indeed

$$\langle \square | \circ \rangle = \frac{1}{d}. \quad (66)$$

Since P is a projector, we used

$$P^2 = P, \quad (67)$$

to apply it also on the initial state matrix. Namely, we defined the averaged initial state matrix as

$$n = \left\langle \begin{array}{c} \text{Diagram: A green circle with two lines extending from its top and bottom, representing the averaged initial state matrix } n. \end{array} \right\rangle = P(m \otimes_r m^*)^{\otimes r^2} P. \quad (68)$$

The above discussion implies that all wires in (62) carry a two-dimensional vector space spanned by $|\circ\rangle$ and $|\square\rangle$. Almost all matrix elements of W and n in this basis are fixed solely by dual unitarity (6) and the normalisation condition (14), and are hence independent on the specific U and m . The only exceptions are

$$\left\langle \begin{array}{c} \text{Diagram: A green square with four lines, two from top and two from bottom, representing a specific matrix element of } W. \end{array} \right\rangle = 1 - p + \frac{p}{d^2}, \quad \left\langle \begin{array}{c} \text{Diagram: A green circle with two lines, one from top and one from bottom, representing a specific matrix element of } n. \end{array} \right\rangle \equiv \frac{c}{d}, \quad (69)$$

where the second equation defines the parameter c , which characterises the averaged initial state matrix. In Appendix B we show that c takes values in $[1, d]$ and it is equal to one only when the initial state is solvable.

Considering for instance the orthonormal bases

$$\{|\circ, \circ\rangle, |\circ, \bullet\rangle, |\bullet, \circ\rangle, |\bullet, \bullet\rangle\}, \quad \{|\circ\rangle, |\bullet\rangle\}, \quad (70)$$

where we introduced the state

$$|\bullet\rangle = \frac{d|\square\rangle - |\circ\rangle}{\sqrt{d^2 - 1}}, \quad (71)$$

we explicitly find

$$W = \begin{bmatrix} 1 & 0 & 0 & 0 \\ 0 & 0 & 1-p & \frac{p}{\sqrt{d^2-1}} \\ 0 & 1-p & 0 & \frac{p}{\sqrt{d^2-1}} \\ 0 & \frac{p}{\sqrt{d^2-1}} & \frac{p}{\sqrt{d^2-1}} & 1 - \frac{2p}{d^2-1} \end{bmatrix}, \quad (72)$$

and

$$n = \begin{bmatrix} 1 & \frac{c-1}{\sqrt{d^2-1}} \\ \frac{c-1}{\sqrt{d^2-1}} & 1 - \frac{2(c-1)}{d^2-1} \end{bmatrix}. \quad (73)$$

Since W bears dependence on the gate only through p , the same holds for \mathcal{P}_x . We also stress that, since the averaged gate is symmetric and parity-invariant, we did not include a mark in its graphical representation.

B. Rigorous Proof of Property 1 for $p \geq \bar{p}(d)$

In this subsection, we make use of the bound (61) to prove Property 1 for $p > \bar{p}(d)$ (cf. (55)). To this end, we introduce the following lemma.

Lemma 1. *For $p \geq \bar{p}(d)$ and any state (13), there exist $A, B \geq 0$ such that*

$$d^x \mathcal{P}_x \leq A + Bx. \quad (74)$$

The choice $B = 0$ can only be made for initial solvable states satisfying (40).

Eq. (74) and (61) imply

$$1 - \frac{\log(A + 2Bt)}{2t \log d} \leq \frac{\bar{S}_A(t)}{4t \log d} \leq 1. \quad (75)$$

Taking the infinite-time limit and using the bound (39), we obtain

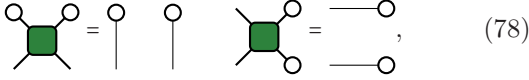
$$v_E = 1, \quad (76)$$

which proves Property 1. Note that using Lemma 1 one can also prove

$$v_{E,\alpha} = 1, \quad \alpha \leq 2, \quad (77)$$

by combining (59), (24) and (35).

To prove Lemma 1 we derive a simple recursive relation for \mathcal{P}_x . We begin by noting that the dual-unitarity conditions (6) imply



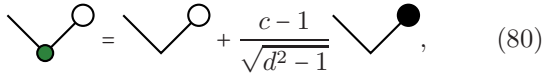
$$\begin{array}{c} \text{○} \quad \text{○} \\ \diagdown \quad / \\ \text{■} \\ \diagup \quad \diagdown \\ \text{—} \quad \text{—} \end{array} = \begin{array}{c} \text{○} \\ | \\ \text{—} \end{array} \quad \begin{array}{c} \text{—} \\ | \\ \text{—} \end{array} \quad \begin{array}{c} \text{—} \\ | \\ \text{—} \end{array} \quad \begin{array}{c} \text{○} \\ | \\ \text{—} \end{array} \quad \begin{array}{c} \text{—} \\ | \\ \text{—} \end{array}, \quad (78)$$

and

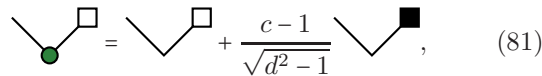


$$\begin{array}{c} \text{□} \quad \text{□} \\ \diagdown \quad / \\ \text{■} \\ \diagup \quad \diagdown \\ \text{—} \quad \text{—} \end{array} = \begin{array}{c} \text{□} \\ | \\ \text{—} \end{array} \quad \begin{array}{c} \text{—} \\ | \\ \text{—} \end{array} \quad \begin{array}{c} \text{—} \\ | \\ \text{—} \end{array} \quad \begin{array}{c} \text{□} \\ | \\ \text{—} \end{array} \quad \begin{array}{c} \text{—} \\ | \\ \text{—} \end{array}. \quad (79)$$

Moreover, we have



$$\begin{array}{c} \text{○} \\ \diagdown \quad / \\ \text{○} \quad \text{■} \end{array} = \begin{array}{c} \text{○} \\ \diagdown \quad / \\ \text{○} \quad \text{○} \end{array} + \frac{c-1}{\sqrt{d^2-1}} \begin{array}{c} \text{—} \\ \diagdown \quad / \\ \text{○} \quad \text{●} \end{array}, \quad (80)$$



$$\begin{array}{c} \text{□} \\ \diagdown \quad / \\ \text{○} \quad \text{■} \end{array} = \begin{array}{c} \text{□} \\ \diagdown \quad / \\ \text{□} \quad \text{○} \end{array} + \frac{c-1}{\sqrt{d^2-1}} \begin{array}{c} \text{—} \\ \diagdown \quad / \\ \text{□} \quad \text{■} \end{array}, \quad (81)$$

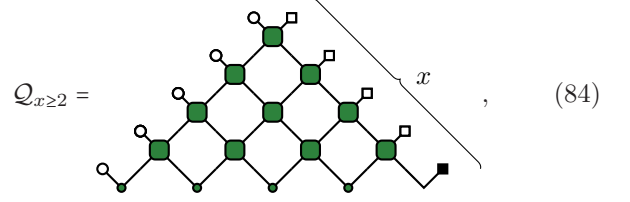
where we introduced

$$\text{■} = \frac{d|\text{○}\rangle - |\text{□}\rangle}{\sqrt{d^2-1}}. \quad (82)$$

We now have all the fundamental ingredients for deriving the desired recursive relations. Using (81) in the bottom right corner of (62), telescoping (79), and using (66) we find

$$\mathcal{P}_x = \frac{1}{d} \mathcal{P}_{x-1} + \frac{c-1}{\sqrt{d^2-1}} \mathcal{Q}_x, \quad (83)$$

where we introduced

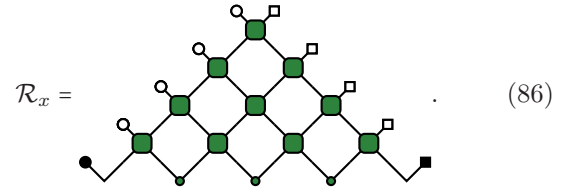


$$\mathcal{Q}_{x \geq 2} = \begin{array}{c} \text{○} \quad \text{□} \\ \diagdown \quad / \\ \text{○} \quad \text{■} \\ \diagup \quad \diagdown \\ \text{○} \quad \text{○} \quad \text{■} \\ \diagdown \quad / \\ \text{○} \quad \text{■} \quad \text{■} \\ \diagup \quad \diagdown \\ \text{○} \quad \text{○} \quad \text{○} \quad \text{■} \\ \diagdown \quad / \\ \text{○} \quad \text{■} \quad \text{■} \quad \text{■} \\ \diagup \quad \diagdown \\ \text{○} \quad \text{○} \quad \text{○} \quad \text{○} \quad \text{■} \\ \diagdown \quad / \\ \text{○} \quad \text{■} \quad \text{■} \quad \text{■} \quad \text{■} \\ \diagup \quad \diagdown \\ \text{○} \quad \text{○} \quad \text{○} \quad \text{○} \quad \text{○} \quad \text{■} \\ \diagdown \quad / \\ \text{○} \quad \text{■} \quad \text{■} \quad \text{■} \quad \text{■} \quad \text{■} \\ \diagup \quad \diagdown \\ \text{○} \quad \text{○} \quad \text{○} \quad \text{○} \quad \text{○} \quad \text{○} \quad \text{■} \\ \diagdown \quad / \\ \text{○} \quad \text{■} \quad \text{■} \quad \text{■} \quad \text{■} \quad \text{■} \quad \text{■} \\ \diagup \quad \diagdown \\ \text{○} \quad \text{○} \quad \text{○} \quad \text{○} \quad \text{○} \quad \text{○} \quad \text{○} \quad \text{■} \\ \diagdown \quad / \\ \text{○} \quad \text{■} \quad \text{■} \quad \text{■} \quad \text{■} \quad \text{■} \quad \text{■} \quad \text{■} \\ \diagup \quad \diagdown \\ \text{○} \quad \text{○} \quad \text{○} \quad \text{○} \quad \text{○} \quad \text{○} \quad \text{○} \quad \text{○} \quad \text{■} \\ \diagdown \quad / \\ \text{○} \quad \text{■} \quad \text{■} \quad \text{■} \quad \text{■} \quad \text{■} \quad \text{■} \quad \text{■} \quad \text{■} \\ \diagup \quad \diagdown \\ \text{○} \quad \text{○} \quad \text{○} \quad \text{○} \quad \text{○} \quad \text{○} \quad \text{○} \quad \text{○} \quad \text{○} \quad \text{■} \\ \diagdown \quad / \\ \text{○} \quad \text{■} \quad \text{■} \quad \text{■} \quad \text{■} \quad \text{■} \quad \text{■} \quad \text{■} \quad \text{■} \quad \text{■} \\ \diagup \quad \diagdown \\ \text{○} \quad \text{○} \quad \text{○} \quad \text{○} \quad \text{○} \quad \text{○} \quad \text{○} \quad \text{○} \quad \text{○} \quad \text{○} \quad \text{■} \\ \diagdown \quad / \\ \text{○} \quad \text{■} \quad \text{■} \quad \text{■} \quad \text{■} \quad \text{■} \quad \text{■} \quad \text{■} \quad \text{■} \quad \text{■} \quad \text{■} \\ \diagup \quad \diagdown \\ \text{○} \quad \text{○} \quad \text{○} \quad \text{○} \quad \text{○} \quad \text{○} \quad \text{○} \quad \text{○} \quad \text{○} \quad \text{○} \quad \text{○} \quad \text{■} \\ \diagdown \quad / \\ \text{○} \quad \text{■} \quad \text{■} \quad \text{■} \quad \text{■} \quad \text{■} \quad \text{■} \quad \text{■} \quad \text{■} \quad \text{■} \quad \text{■} \quad \text{■} \\ \diagup \quad \diagdown \\ \text{○} \quad \text{○} \quad \text{○} \quad \text{○} \quad \text{○} \quad \text{○} \quad \text{○} \quad \text{○} \quad \text{○} \quad \text{○} \quad \text{○} \quad \text{○} \quad \text{■} \\ \diagdown \quad / \\ \text{○} \quad \text{■} \quad \text{■} \quad \text{■} \quad \text{■} \quad \text{■} \quad \text{■} \quad \text{■} \quad \text{■} \quad \text{■} \quad \text{■} \quad \text{■} \quad \text{■} \\ \diagup \quad \diagdown \\ \text{○} \quad \text{○} \quad \text{○} \quad \text{○} \quad \text{○} \quad \text{○} \quad \text{○} \quad \text{○} \quad \text{○} \quad \text{○} \quad \text{○} \quad \text{○} \quad \text{○} \quad \text{■} \\ \diagdown \quad / \\ \text{○} \quad \text{■} \quad \text{■} \quad \text{■} \quad \text{■} \quad \text{■} \quad \text{■} \quad \text{■} \quad \text{■} \quad \text{■} \quad \text{■} \quad \text{■} \quad \text{■} \quad \text{■} \\ \diagup \quad \diagdown \\ \text{○} \quad \text{○} \quad \text{○} \quad \text{○} \quad \text{○} \quad \text{○} \quad \text{○} \quad \text{○} \quad \text{○} \quad \text{○} \quad \text{○} \quad \text{○} \quad \text{○} \quad \text{○} \quad \text{■} \\ \diagdown \quad / \\ \text{○} \quad \text{■} \quad \text{■} \quad \text{■} \quad \text{■} \quad \text{■} \quad \text{■} \quad \text{■} \quad \text{■} \quad \text{■} \quad \text{■} \quad \text{■} \quad \text{■} \quad \text{■} \quad \text{■} \\ \diagup \quad \diagdown \\ \text{○} \quad \text{○} \quad \text{○} \quad \text{○} \quad \text{○} \quad \text{○} \quad \text{○} \quad \text{○} \quad \text{○} \quad \text{○} \quad \text{○} \quad \text{○} \quad \text{○} \quad \text{○} \quad \text{○} \quad \text{■} \\ \diagdown \quad / \\ \text{○} \quad \text{■} \quad \text{■} \quad \text{■} \quad \text{■} \quad \text{■} \quad \text{■} \quad \text{■} \quad \text{■} \quad \text{■} \quad \text{■} \quad \text{■} \quad \text{■} \quad \text{■} \quad \text{■} \quad \text{■} \\ \diagup \quad \diagdown \\ \text{○} \quad \text{○} \quad \text{○} \quad \text{○} \quad \text{○} \quad \text{○} \quad \text{○} \quad \text{○} \quad \text{○} \quad \text{○} \quad \text{○} \quad \text{○} \quad \text{○} \quad \text{○} \quad \text{○} \quad \text{○} \quad \text{■} \\ \diagdown \quad / \\ \text{○} \quad \text{■} \quad \text{■} \quad \text{■} \quad \text{■} \quad \text{■} \quad \text{■} \quad \text{■} \quad \text{■} \quad \text{■} \quad \text{■} \quad \text{■} \quad \text{■} \quad \text{■} \quad \text{■} \quad \text{■} \quad \text{■} \\ \diagup \quad \diagdown \\ \text{○} \quad \text{○} \quad \text{○} \quad \text{○} \quad \text{○} \quad \text{○} \quad \text{○} \quad \text{○} \quad \text{○} \quad \text{○} \quad \text{○} \quad \text{○} \quad \text{○} \quad \text{○} \quad \text{○} \quad \text{○} \quad \text{○} \quad \text{■} \\ \diagdown \quad / \\ \text{○} \quad \text{■} \quad \text{■} \quad \text{■} \quad \text{■} \quad \text{■} \quad \text{■} \quad \text{■} \quad \text{■} \quad \text{■} \quad \text{■} \quad \text{■} \quad \text{■} \quad \text{■} \quad \text{■} \quad \text{■} \quad \text{■} \quad \text{■} \\ \diagup \quad \diagdown \\ \text{○} \quad \text{○} \quad \text{○} \quad \text{○} \quad \text{○} \quad \text{○} \quad \text{○} \quad \text{○} \quad \text{○} \quad \text{○} \quad \text{○} \quad \text{○} \quad \text{○} \quad \text{○} \quad \text{○} \quad \text{○} \quad \text{○} \quad \text{○} \quad \text{■} \\ \diagdown \quad / \\ \text{○} \quad \text{■} \quad \text{■} \quad \text{■} \quad \text{■} \quad \text{■} \quad \text{■} \quad \text{■} \quad \text{■} \quad \text{■} \quad \text{■} \quad \text{■} \quad \text{■} \quad \text{■} \quad \text{■} \quad \text{■} \quad \text{■} \quad \text{■} \quad \text{■} \\ \diagup \quad \diagdown \\ \text{○} \quad \text{■} \\ \diagdown \quad / \\ \text{○} \quad \text{■} \end{array}, \quad (84)$$

and $\mathcal{Q}_1 = \langle \text{○} | \text{■} \rangle = \sqrt{d^2-1}/d$. Applying now (80) to the bottom left corner of (84) and then telescoping (78), we have

$$\mathcal{Q}_x = \frac{1}{d} \mathcal{Q}_{x-1} + \frac{c-1}{\sqrt{d^2-1}} \mathcal{R}_x, \quad (85)$$

where



$$\mathcal{R}_x = \begin{array}{c} \text{○} \quad \text{□} \\ \diagdown \quad / \\ \text{○} \quad \text{■} \\ \diagup \quad \diagdown \\ \text{○} \quad \text{○} \quad \text{■} \\ \diagdown \quad / \\ \text{○} \quad \text{■} \quad \text{■} \\ \diagup \quad \diagdown \\ \text{○} \quad \text{○} \quad \text{○} \quad \text{■} \\ \diagdown \quad / \\ \text{○} \quad \text{■} \quad \text{■} \quad \text{■} \\ \diagup \quad \diagdown \\ \text{○} \quad \text{○} \quad \text{○} \quad \text{○} \quad \text{■} \\ \diagdown \quad / \\ \text{○} \quad \text{■} \quad \text{■} \quad \text{■} \quad \text{■} \\ \diagup \quad \diagdown \\ \text{○} \quad \text{○} \quad \text{○} \quad \text{○} \quad \text{○} \quad \text{■} \\ \diagdown \quad / \\ \text{○} \quad \text{■} \quad \text{■} \quad \text{■} \quad \text{■} \quad \text{■} \\ \diagup \quad \diagdown \\ \text{○} \quad \text{○} \quad \text{○} \quad \text{○} \quad \text{○} \quad \text{○} \quad \text{■} \\ \diagdown \quad / \\ \text{○} \quad \text{■} \quad \text{■} \quad \text{■} \quad \text{■} \quad \text{■} \quad \text{■} \\ \diagup \quad \diagdown \\ \text{○} \quad \text{○} \quad \text{○} \quad \text{○} \quad \text{○} \quad \text{○} \quad \text{○} \quad \text{■} \\ \diagdown \quad / \\ \text{○} \quad \text{■} \quad \text{■} \quad \text{■} \quad \text{■} \quad \text{■} \quad \text{■} \quad \text{■} \\ \diagup \quad \diagdown \\ \text{○} \quad \text{○} \quad \text{○} \quad \text{○} \quad \text{○} \quad \text{○} \quad \text{○} \quad \text{○} \quad \text{■} \\ \diagdown \quad / \\ \text{○} \quad \text{■} \quad \text{■} \quad \text{■} \quad \text{■} \quad \text{■} \quad \text{■} \quad \text{■} \quad \text{■} \\ \diagup \quad \diagdown \\ \text{○} \quad \text{○} \quad \text{○} \quad \text{○} \quad \text{○} \quad \text{○} \quad \text{○} \quad \text{○} \quad \text{○} \quad \text{■} \\ \diagdown \quad / \\ \text{○} \quad \text{■} \quad \text{■} \quad \text{■} \quad \text{■} \quad \text{■} \quad \text{■} \quad \text{■} \quad \text{■} \quad \text{■} \quad \text{■} \end{array}. \quad (86)$$

To close the recursive system formed by (83) and (85), we now seek a bound for \mathcal{R}_x . In particular, a bound of the form

$$|\mathcal{R}_x| \leq \frac{C}{D^x}, \quad (87)$$

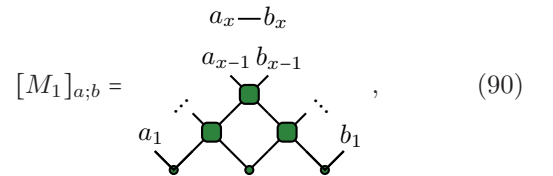
for some $C > 0$ and $D > d$, leads to

$$\mathcal{Q}_x \leq \frac{\alpha}{d^x} + \frac{\beta}{D^x}, \quad (88)$$

$$\mathcal{P}_x \leq \frac{\gamma}{d^x} + \frac{(c-1)\alpha}{\sqrt{d^2-1}} \frac{x}{d^x} + \frac{\delta}{D^x}, \quad \alpha, \beta, \gamma, \delta \in \mathbb{R}, \quad (89)$$

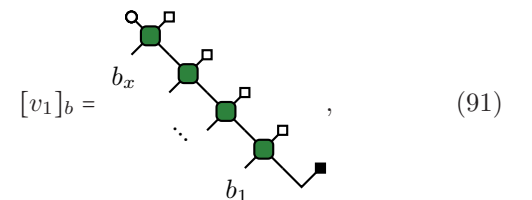
which immediately imply (74).

To find the bound in Eq. (87), we view \mathcal{R}_x as the matrix element of



$$[M_1]_{a;b} = \begin{array}{c} a_x - b_x \\ \diagdown \quad / \\ a_{x-1} \quad b_{x-1} \\ \diagup \quad \diagdown \\ \vdots \quad \vdots \\ a_1 \quad \vdots \quad b_1 \end{array}, \quad (90)$$

between the vectors



$$[v_1]_b = \begin{array}{c} b_x \\ \diagdown \quad / \\ \vdots \\ b_1 \end{array}, \quad (91)$$

and

$$[w_1]_a = \begin{array}{c} \text{---} a_x \\ \diagup \quad \diagdown \\ \text{---} a_{x-1} \\ \diagup \quad \diagdown \\ \text{---} a_1 \end{array} \quad (92)$$

Employing the Cauchy-Schwartz inequality, we then obtain

$$|\mathcal{R}_x| = |\langle v_1 | M_1 | w_1 \rangle| \leq \|M_1\|_\infty \sqrt{\langle v_1 | v_1 \rangle} \sqrt{\langle w_1 | w_1 \rangle}. \quad (93)$$

Let us now consider separately the three factors on the r.h.s.. Since the gates are the average of dual-unitary gates, the operator norm of the dual averaged gate \tilde{W} , with elements

$$[\tilde{W}]_{(ab);(cd)} \equiv \begin{array}{c} b \quad d \\ \diagdown \quad \diagup \\ \text{---} \\ \diagup \quad \diagdown \\ a \quad c \end{array}, \quad (94)$$

is one. Therefore, we have nontrivial contributions to the norm of M_1 only from the initial state row. This gives

$$\|M_1\|_\infty = \|n\|_\infty^{x-2} = \left(\frac{d+c}{d+1}\right)^{x-2}, \quad (95)$$

where the identity

$$\|n\|_\infty = \frac{d+c}{d+1}, \quad (96)$$

is proven in Appendix B.

Eq. (95) is the *key simplification* provided by dual-unitarity in the current setting. Even though the boundary conditions at the bottom of the tensor network (90) are generic, dual-unitarity implies that its operator norm scales with the number of tensors on its edge. This should be contrasted with the non-dual-unitary case, where the dual gate \tilde{W} has operator norm greater than one [86], and, therefore, the operator norm of M_1 scales with the total number of tensors composing it. In summary, because of dual-unitarity, Eq. (95) shows an ‘‘area scaling’’ rather than a ‘‘volume scaling’’. As we now see, for large enough entangling power p such an area scaling can be counter-balanced by the other two terms in (93), leading to the bound (87).

To treat the second factor in (93) we introduce the matrix

$$T_2 = \begin{array}{c} \text{---} \\ \diagdown \quad \diagup \\ \text{---} \\ \diagup \quad \diagdown \\ \text{---} \\ \diagdown \quad \diagup \\ \text{---} \\ \diagup \quad \diagdown \\ \text{---} \end{array} \quad (97)$$

so that we can write

$$\langle v_1 | v_1 \rangle = \left. \begin{array}{c} \text{---} \\ \diagdown \quad \diagup \\ \text{---} \\ \diagup \quad \diagdown \\ \text{---} \\ \diagdown \quad \diagup \\ \text{---} \\ \diagup \quad \diagdown \\ \text{---} \end{array} \right\} x-1 = \langle \text{---} | T_2^{x-1} | \text{---} \rangle, \quad (98)$$

where we used the fact that the averaged gate is real. As shown in Appendix C, the vector $|\text{---}\rangle$ is an eigenvector of T_2 with eigenvalue

$$\lambda(p) = (1-p)^2 + \frac{p^2}{d^2-1}. \quad (99)$$

Therefore, we have

$$\langle v_1 | v_1 \rangle = \lambda(p)^{x-1} \langle \text{---} | \text{---} \rangle = \lambda(p)^{x-1} \frac{d^2-1}{d^2}. \quad (100)$$

Proceeding analogously (cf. Appendix C) we find

$$\langle w_1 | w_1 \rangle = \lambda(p)^{x-2}. \quad (101)$$

Finally, putting all together, we obtain the following bound

$$|\mathcal{R}_x| \leq \left(\frac{d+1}{d+c}\right)^2 \sqrt{\frac{d^2-1}{d^2\lambda(p)^3}} \left(\frac{d+c}{d+1}\right)^x \lambda(p)^x \quad (102)$$

$$\leq \left(\frac{d+1}{d+c}\right)^2 \sqrt{\frac{d^2-1}{d^2\lambda(p)^3}} \left(\frac{2d}{d+1}\right)^x \lambda(p)^x, \quad (103)$$

where we used that $c \leq d$. Choosing p such that

$$\lambda(p) \frac{2d}{d+1} < \frac{1}{d}, \quad (104)$$

we then find the bound (87). Solving for p we find that (104) is indeed satisfied for all

$$p \geq \bar{p}(d). \quad (105)$$

This concludes the proof.

C. Extension to $p < \bar{p}(d)$

An obvious strategy to generalise our proof is to extend Lemma 1 to $p \leq \bar{p}(d)$. To this end, a simple observation is that, for small enough values of c , one can use the tighter bound (102) for $|\mathcal{R}_x|$. The latter grants the validity of Lemma 1 whenever

$$\left(\frac{d+c}{d+1}\right) \lambda(p) < \frac{1}{d}. \quad (106)$$

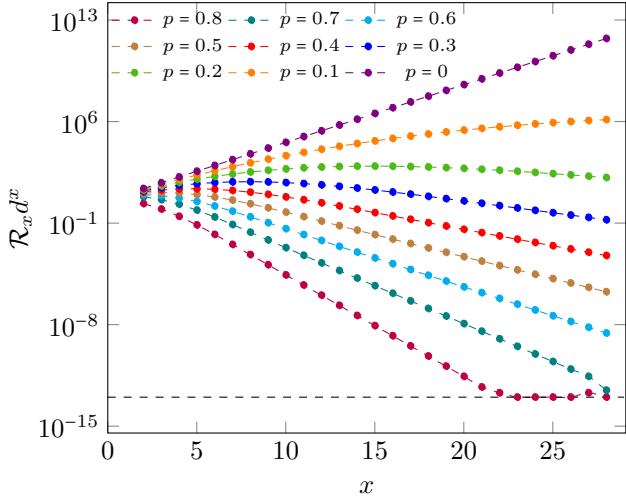


FIG. 1. Remainder $d^x \mathcal{R}_x$ (cf. (86)) for $c = 2.5$, $d = 5$, and several values of p . The exponential decay (87) with $D > d$ covers much more values than the range $p \gtrsim 0.62$, for which our rigorous bound (106) applies. The dotted line on the bottom indicates the limit of the numerical accuracy.

Recalling that $c \geq 1$ (cf. Appendix B) we find that this bound can be satisfied for some c only if

$$p > \tilde{p}(d) \equiv \frac{d^2 - 1}{d^2} \left(1 - \frac{1}{\sqrt{d+1}} \right). \quad (107)$$

In fact, the bound (106) can be easily refined. For instance, instead of Eq. (93) we can consider

$$|\mathcal{R}_x| \leq \sqrt{\langle w_2 | w_2 \rangle} \sqrt{\langle v_2 | v_2 \rangle} \|M_2\|, \quad (108)$$

with $|w_2\rangle, |v_2\rangle$, defined with an extra row of gates, i.e.

$$v_2 = \text{[Circuit Diagram]} \quad (109)$$

Comparing this with (91), we see that the norm $\langle v_2 | v_2 \rangle$ involves the matrix T_4 . One can directly verify that the eigenvalue of T_4 contributing to this norm corresponds to an eigenvector with support 4 and it is strictly smaller than $\lambda(p)$. This results in an immediate improvement of the bound. In fact, this procedure can be repeated considering increasingly “thicker” states $|w_x\rangle, |v_x\rangle$ for any $x \geq 2$ and leads to a systematic improvement.

The fact that the bound on \mathcal{R}_x can be improved is also suggested by numerical evidence. For instance, in Figure 1 we show the behaviour of $\mathcal{R}_x d^x$ as a function of time for $d = 5$. We see that the exponential decay (87) — which implies the validity of Lemma 1 — is clearly shown

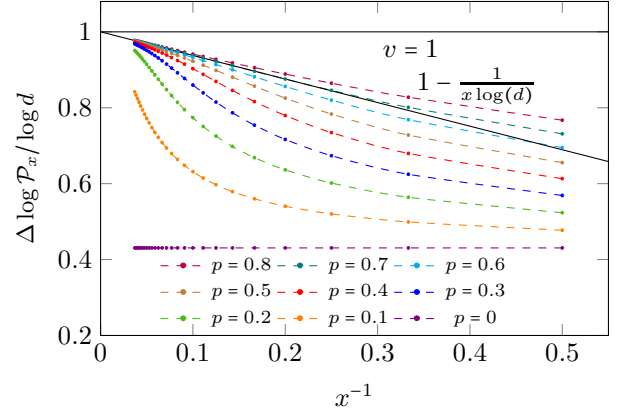


FIG. 2. Increment of the indicator $\Delta \log(\mathcal{P}_x)$ in Eq. (110) per step for an initial state corresponding to $c = 2.5$ and $d = 5$. The quantity is expected to saturate at the averaged velocity value as $x \rightarrow \infty$. Note that our rigorous analytic bound (106) applies only if $p \gtrsim 0.62$. Assuming $d^x \mathcal{P}_x \sim A + Bx$ even for $p > 0.62$, we expect, for large x , $\Delta \log \mathcal{P}_x \sim 1 - 1/(x \log d)$.

by our numerical evaluations for $p > 0.3$, which should be compared with $\bar{p}(5) \approx 0.68$ and $\tilde{p}(5) \approx 0.57$. From the trend in the numerical data, it is reasonable to expect that, upon accessing larger values of x , the same decay would be observed for all $p \neq 0$. A different indication is shown in Figure 2, which suggests that

$$\Delta \log \mathcal{P}_x \equiv \log \mathcal{P}_{x-1} - \log \mathcal{P}_x, \quad (110)$$

approaches 1 for all values of p except for a neighbourhood of $p = 0$. Consistently with Lemma 1 the leading corrections at large x appear to be $\approx x^{-1}$.

D. Numerical results for single realisations

In this subsection we provide numerical evidence supporting the claim that v_E is maximal for essentially *any* single realisation of the gates (47). For our numerical experiments we consider dual-unitary quantum circuits with a 2-dimensional local Hilbert space. In this case the most general local gate can be written as

$$U_{(ab);(cd)} = \sum_{a',b'=1}^2 \exp(iJ\delta_{a'b'}) u_{+a;a'} u_{-b;b'} v_{+c;b'} v_{-d;a'}, \quad (111)$$

where $\{v_{\pm}, u_{\pm}\}$ are fixed $U(2)$ matrices and $J \in [0, \pi/2]$. The angle J is in one-to-one correspondence with the entangling power [57]. Specifically, using the definition (8) we have

$$p = \frac{2}{3} \cos(J)^2. \quad (112)$$

In the following we use p , rather than J , to keep consistency with the previous subsections. The initial state matrix is instead taken of the form

$$m_{a;b} = (1 - \delta_{ab}) \sin(\theta) + \delta_{ab} \cos \theta. \quad (113)$$

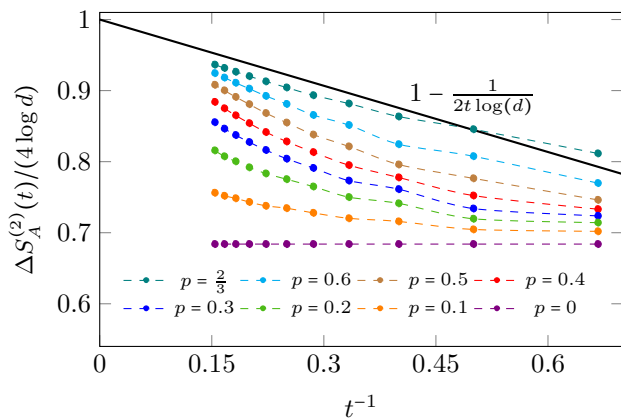


FIG. 3. $\Delta S_A^{(2)}(t)$ as a function of t^{-1} for a system prepared in a generic pair product state specified by the matrices (113) with $\theta = 0.35$ and evolved with a homogeneous dual-unitary quantum circuit with local gate (111), with fixed $\{v_{\pm}, u_{\pm}\}$ (their explicit form is reported in Appendix D) and different values of a (related to J through (112)). This quantity saturates at the Rényi-2 entanglement velocity $v_{E,2}$ as $t \rightarrow \infty$. Assuming that for large times $S_A^{(2)}(t) \sim -2 \log \mathcal{P}_{2t}$, we expect the various plots to reach asymptotically the line $1 - 1/(2t \log(d))$ (black).

Focussing on a space-time translationally invariant circuit, i.e., a circuit where the local gate is the same at each space-time point, we compute the Rényi entropy $S_A^{(2)}(t)$ for $t \leq L_A/2$ by numerically constructing the matrix C_x (cf. (30)) and using (32). This direct approach allows us to reach values of x up to 14. Note that, due to the fast growth of entanglement in dual-unitary circuits, this is more efficient than tensor network methods based on the truncation of the time-evolving state, e.g., TEBD.

A representative example of our results is presented in Figure 3, where we report $\Delta S_A^{(2)}(t)$ (cf. Eq. (44)) as a function of the inverse time. Our results suggest that at large times $\Delta S_A^{(2)}(t)$ approaches $4 \log d$ with power law corrections that, as observed in the averaged case, are larger for smaller values of p . This implies

$$v_{E,2} = v_E = 1, \quad (114)$$

in accordance with our expectations.

V. DISCUSSION

We studied the asymptotic growth of entanglement in dual-unitary circuits prepared in generic two-site product states. These states are generally *non-solvable*: they break the unitarity of the evolution in space and their entanglement dynamics cannot be accessed using the standard dual-unitarity-based approaches [25, 26]. Moreover, as opposed to solvable states, they display a sub-maximal entanglement increment at short times.

By introducing dual-unitarity-preserving random noise we showed that, surprisingly, the entanglement dynamics

of generic states remain *exactly tractable* for large times: one can still make exact statements for individual realisations of the noise, possibly excluding a subset with zero measure. In this way we proved that for a class of dual-unitary circuits with large enough entangling power the growth-rate of entanglement approaches the maximal value as time increases — i.e. their entanglement velocity is always maximal irrespective of the initial conditions. We showed that this maximally entangling class exists for any number d of local degrees of freedom as it includes the Hadamard family of dual-unitary gates introduced in Ref. [72]. Moreover, for $d \geq 3$ it also contains 4-leg perfect tensors [73, 74, 81–83]. In fact, we presented analytical and numerical arguments suggesting that all dual-unitary circuits with non-zero entangling power belong to this class.

Our results established an even tighter connection between dual-unitarity and maximal entanglement growth. While Ref. [71] recently showed that if there exists an initial state for which the asymptotic entanglement rate is maximal, then the circuit is dual unitary, here we showed that in generic dual-unitary circuits *every* initial state eventually approaches maximal entanglement growth. In this respect, our results show that dual-unitary circuits are the hardest quantum circuits to simulate with classical computers [34–37] making of them the optimal test bed for investigations on quantum supremacy in the non-equilibrium dynamics [87].

A natural question is whether our “generality” assumption — the fact that we excluded a zero-measure set of gates — is necessary or not. Namely, do we need to exclude some special dual-unitary gates (e.g. the integrable ones) or *any* dual-unitary circuit generates maximal entanglement growth at large times? This would establish whether dual-unitarity is sufficient to produce initial-condition independent entanglement velocities or one also needs quantum chaos.

Finally, we stress that the methods developed here provide a systematic way to investigate quenches from generic initial states in dual-unitary circuits. Interesting questions that one can tackle with them include (deep) thermalization timescales in dual-unitary circuits [25, 26, 65, 70], and multi-unital quantum channels [88], or the “temporal entanglement” scaling in chaotic quantum circuits [89] (see also Refs. [77, 90–92]). The latter question is currently under investigation [93].

ACKNOWLEDGMENTS

We thank Tianci Zhou for collaboration on a closely related project and for many useful comments on the manuscript. We also grateful to Lorenzo Piroli, Tomaz Prosen, Pavel Kos, and, especially, Katja Klobas for very valuable feedback on the manuscript. This work has been supported by the Royal Society through the University Research Fellowship No. 201101.

Appendix A: Bounds on the entangling power of dual-unitary gates

The values that the entangling power p can take are bounded by the unitarity of the matrix. To see this, consider $\text{tr}[(\tilde{U}^{t_2}(\tilde{U}^{t_2})^\dagger)^2]$ in the definition (8): the unitarity of the matrix fixes the value of

$$\text{tr}[\tilde{U}^{t_2}(\tilde{U}^{t_2})^\dagger] = \text{tr}[\tilde{U}\tilde{U}^\dagger] = d^2. \quad (\text{A1})$$

Applying (34) to the matrix $\frac{\tilde{U}^{t_2}(\tilde{U}^{t_2})^\dagger}{d^2}$, we find

$$\text{tr}[(\tilde{U}^{t_2}(\tilde{U}^{t_2})^\dagger)^2] \in [d^2, d^4] \implies p \in [0, 1]. \quad (\text{A2})$$

In particular, the case

$$\text{tr}[(\tilde{U}^{t_2}(\tilde{U}^{t_2})^\dagger)^2] = d^2 \quad (\text{A3})$$

is attained if and only if \tilde{U}^{t_2} is unitary, having all eigenvalues with magnitude 1. This request, together with the dual unitarity conditions (6), means that U is unitary for any choice of couples of in/out indexes. Tensors with this property are known as 4-leg perfect tensors and they exist for all $d > 2$ [73, 74]. There is, however, a non-exhaustive class of dual unitary gates which is well defined in any dimension [62]

$$U_{(ab),(cd)} = \delta_{ad}\delta_{bc} \exp(iJ_{ab}), \quad (\text{A4})$$

with J_{ab} being any set of d^2 real numbers. In terms of J_{ab} , we can write

$$\text{tr}[(\tilde{U}^{t_2}(\tilde{U}^{t_2})^\dagger)^2] = \sum_{a,b,c,d} \exp[i(J_{ab} + J_{cd} - J_{ad} - J_{cb})]. \quad (\text{A5})$$

As before, we can express the right-hand side as a matrix trace

$$\sum_{a,b,c,d} \exp[i(J_{ab} + J_{cd} - J_{ad} - J_{cb})] = d^4 \text{tr}[(\xi\xi^\dagger)^2], \quad (\text{A6})$$

with

$$\xi_{ab} \equiv \frac{\exp(iJ_{ab})}{d} \implies \text{Tr}[\xi\xi^\dagger] = 1. \quad (\text{A7})$$

Using again (34), we find

$$\text{tr}[(\tilde{U}^{t_2}(\tilde{U}^{t_2})^\dagger)^2] \in [d^3, d^4] \implies p \in \left[0, \frac{d}{d+1}\right]. \quad (\text{A8})$$

The choice $J_{ab} = 0$, which corresponds to a swap gate, gives $p = 0$. Instead, the choice

$$J_{ab} = \frac{2\pi ab}{d}, \quad (\text{A9})$$

corresponding to the Hadamard family considered in Section IV, gives

$$p = \frac{d}{d+1}. \quad (\text{A10})$$

We also note that, since the value of p depends continuously on J_{ab} , there must exist gates corresponding to all values in the range

$$p \in \left[0, \frac{d}{d+1}\right]. \quad (\text{A11})$$

Finally, we remark that this range is exhaustive in $d = 2$, since any dual unitary gate can be expressed as in Eq. (111).

Appendix B: Averaged initial state matrix

Considering the averaged form of the initial state matrix in the basis $\{|\circ\rangle, |\bullet\rangle\}$ we have

$$n = \begin{pmatrix} 1 & \frac{c-1}{\sqrt{d^2-1}} \\ \frac{c-1}{\sqrt{d^2-1}} & 1 - 2\frac{c-1}{d^2-1} \end{pmatrix}, \quad (\text{B1})$$

with

$$c = \frac{1}{d} \text{tr}((m^\dagger m)^2). \quad (\text{B2})$$

We can bound the values that the constant c can take noting that the matrix m is subject to the constraint

$$\text{tr}(m^\dagger m) = d. \quad (\text{B3})$$

Therefore, we can use (34) on $m^\dagger m / d$ with $\mathcal{N} = d$, $\alpha = 2$, finding

$$c \in [1, d]. \quad (\text{B4})$$

The matrix (B1) is Hermitian and, therefore, its operator norm coincides with the norm of its maximal eigenvalue. Computing it explicitly, we find

$$\begin{aligned} \lambda_{max} &= 1 - \frac{c-1}{d^2-1} + \sqrt{\left(\frac{c-1}{\sqrt{d^2-1}}\right)^2 + \left(\frac{c-1}{d^2-1}\right)^2} \\ &= 1 - \frac{c-1}{d^2-1} \left(1 - \sqrt{d^2-1} + 1\right) = \frac{d+c}{d+1}. \end{aligned} \quad (\text{B5})$$

In summary we have

$$\|n\|_\infty = \frac{c+d}{d+1} \in \left[1, \frac{2d}{d+1}\right]. \quad (\text{B6})$$

Appendix C: Two-site transfer matrix

Consider the transfer matrix T_2 in Eq. (97): using the explicit expression for the averaged gate (72) (which has the same form in the square states basis), we see that its explicit form in the basis

$$\{|\square\square\rangle, |\blacksquare\square\rangle, |\square\blacksquare\rangle, |\blacksquare\blacksquare\rangle\}, \quad (\text{C1})$$

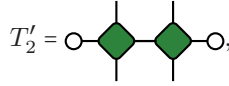
reads as

$$T_2 = \begin{pmatrix} 1 & 0 & 0 & 0 \\ 0 & 1-p & 0 & 0 \\ 0 & 0 & 1-p & 0 \\ 0 & 0 & 0 & (1-p)^2 + \frac{p^2}{d^2-1} \end{pmatrix}, \quad (\text{C2})$$

allowing us to immediately compute

$$\begin{aligned} \langle v_2 | v_2 \rangle &= \langle \text{OO} | T_2^{x-1} | \blacksquare\blacksquare \rangle \\ &= \lambda(p)^{x-1} \langle \text{OO} | \blacksquare\blacksquare \rangle = \\ &= \lambda(p)^{x-1} \frac{d^2-1}{d^2}. \end{aligned} \quad (\text{C3})$$

Similarly, the transfer matrix

$$T'_2 = \text{O} \text{---} \text{O} \text{---} \text{O}, \quad (\text{C4})$$


can be put in the same form under a unitary change of basis $\{\blacksquare, \blacksquare\} \rightarrow \{\text{O}, \bullet\}$, allowing us to find

$$\begin{aligned} \langle w_2 | w_2 \rangle &= \langle \bullet\bullet | T'^{x-2} | \text{O} \rangle \\ &= \lambda(p)^{x-2} \langle \bullet\bullet | \text{O} \rangle \\ &= \lambda(p)^{x-2}, \end{aligned} \quad (\text{C5})$$

where we used the notation for the arc state

$$|\text{O}\rangle = |\text{OO}\rangle + |\bullet\bullet\rangle. \quad (\text{C6})$$

Appendix D: Details of the numerics

In Fig. 3 we plotted the numerical evaluation of the Rényi 2 entropy for different values of the parameter p . We implemented the gates defined in Eq. (111), where the unitary matrices $u_{\pm}, v_{\pm} \in U(2)$ are obtained from a random Haar uniform extraction. Those matrices are kept fixed while varying the value of J (or p , which are connected through Eq. (112)). The explicit parameterization implemented is the following

$$\begin{bmatrix} \cos(\alpha) + i \sin(\alpha) \cos(\theta) & i \sin(\alpha) \sin(\theta) e^{-i\phi} \\ i \sin(\alpha) \sin(\theta) e^{i\phi} & \cos(\alpha) - i \sin(\alpha) \cos(\theta) \end{bmatrix}. \quad (\text{D1})$$

The values used to produce Fig. 3 are reported in Tab. I.

	θ	ϕ	α
u_{-}	0.774764	5.531527	4.534001
u_{+}	2.521203	3.352128	4.712387
v_{-}	1.768693	0.704289	5.567499
v_{+}	0.251880	1.607363	5.823117

TABLE I. Parameters for the one-site unitaries used to produce the data in Figure 3.

-
- [1] L. Amico, R. Fazio, A. Osterloh, and V. Vedral, Entanglement in many-body systems, *Rev. Mod. Phys.* **80**, 517 (2008).
- [2] P. Calabrese, J. Cardy, and B. Doyon, Entanglement entropy in extended quantum systems, *J. Phys. A: Math. Theor.* **42**, 500301 (2009).
- [3] P. Calabrese, Entanglement and thermodynamics in non-equilibrium isolated quantum systems, *Physica A* **504**, 31 (2018).
- [4] N. Laflorencie, Quantum entanglement in condensed matter systems, *Phys. Rep.* **646**, 1 (2016).
- [5] P. Calabrese and J. Cardy, Evolution of entanglement entropy in one-dimensional systems, *J. Stat. Mech.: Theory Exp.* **2005** (04), P04010.
- [6] A. Nahum, J. Ruhman, S. Vijay, and J. Haah, Quantum entanglement growth under random unitary dynamics, *Phys. Rev. X* **7**, 031016 (2017).
- [7] J. M. Deutsch, H. Li, and A. Sharma, Microscopic origin of thermodynamic entropy in isolated systems, *Phys. Rev. E* **87**, 042135 (2013).
- [8] W. Beugeling, A. Andreanov, and M. Haque, Global characteristics of all eigenstates of local many-body hamiltonians: participation ratio and entanglement entropy, *J. Stat. Mech.: Theory and Exp.* **2015**, P02002 (2015).
- [9] V. Gurarie, Global large time dynamics and the generalized gibbs ensemble, *J. Stat. Mech.: Theory and Exp.* **2013**, P02014 (2013).
- [10] V. Alba and P. Calabrese, Entanglement and thermodynamics after a quantum quench in integrable systems, *Proc. Natl. Acad. Sci. U.S.A.* **114**, 7947 (2017).
- [11] G. D. Chiara, S. Montangero, P. Calabrese, and R. Fazio, Entanglement entropy dynamics of Heisenberg chains, *J. Stat. Mech.: Theory Exp.* **2006** (03), P03001.
- [12] M. Žnidarič, T. Prosen, and P. Prelovšek, Many-body localization in the Heisenberg XXZ magnet in a random field, *Phys. Rev. B* **77**, 064426 (2008).
- [13] R. Nandkishore and D. A. Huse, Many-body localization and thermalization in quantum statistical mechanics, *Annu. Rev. Condens. Matter Phys.* **6**, 15 (2015).
- [14] M. Kormos, M. Collura, G. Takács, and P. Calabrese, Real-time confinement following a quantum quench to a non-integrable model, *Nat. Phys.* **13**, 246 (2017).
- [15] B. Skinner, J. Ruhman, and A. Nahum, Measurement-induced phase transitions in the dynamics of entanglement, *Phys. Rev. X* **9**, 031009 (2019).
- [16] Y. Li, X. Chen, and M. P. A. Fisher, Measurement-driven entanglement transition in hybrid quantum circuits, *Phys. Rev. B* **100**, 134306 (2019).
- [17] R. Vasseur, A. C. Potter, Y.-Z. You, and A. W. W. Ludwig, Entanglement transitions from holographic random

- tensor networks, *Phys. Rev. B* **100**, 134203 (2019).
- [18] M. Fagotti and P. Calabrese, Evolution of entanglement entropy following a quantum quench: Analytic results for the XY chain in a transverse magnetic field, *Phys. Rev. A* **78**, 010306 (2008).
- [19] B. Bertini, E. Tartaglia, and P. Calabrese, Entanglement and diagonal entropies after a quench with no pair structure, *J. Stat. Mech.: Theory Exp.* **2018** (6), 063104.
- [20] V. Alba and P. Calabrese, Entanglement dynamics after quantum quenches in generic integrable systems, *SciPost Phys.* **4**, 17 (2018).
- [21] G. Lagnese, P. Calabrese, and L. Piroli, Entanglement dynamics of thermofield double states in integrable models, [2112.02008](https://arxiv.org/abs/2112.02008) (2021), arXiv:2112.02008.
- [22] A. M. Läuchli and C. Kollath, Spreading of correlations and entanglement after a quench in the one-dimensional bose-hubbard model, *J. Stat. Mech.: Theory Exp.* **2008** (05), P05018.
- [23] H. Kim and D. A. Huse, Ballistic spreading of entanglement in a diffusive nonintegrable system, *Phys. Rev. Lett.* **111**, 127205 (2013).
- [24] R. Pal and A. Lakshminarayan, Entangling power of time-evolution operators in integrable and nonintegrable many-body systems, *Phys. Rev. B* **98**, 174304 (2018).
- [25] B. Bertini, P. Kos, and T. Prosen, Entanglement spreading in a minimal model of maximal many-body quantum chaos, *Phys. Rev. X* **9**, 021033 (2019).
- [26] L. Piroli, B. Bertini, J. I. Cirac, and T. Prosen, Exact dynamics in dual-unitary quantum circuits, *Phys. Rev. B* **101**, 094304 (2020).
- [27] S. Gopalakrishnan and A. Lamacraft, Unitary circuits of finite depth and infinite width from quantum channels, *Phys. Rev. B* **100**, 064309 (2019).
- [28] T. Zhou and A. Nahum, Entanglement membrane in chaotic many-body systems, *Phys. Rev. X* **10**, 031066 (2020).
- [29] H. Liu and S. J. Suh, Entanglement tsunami: Universal scaling in holographic thermalization, *Phys. Rev. Lett.* **112**, 011601 (2014).
- [30] C. T. Asplund, A. Bernamonti, F. Galli, and T. Hartman, Entanglement scrambling in 2d conformal field theory, *J. High Energy Phys.* **2015** (9), 110.
- [31] C. W. von Keyserlingk, T. Rakovszky, F. Pollmann, and S. L. Sondhi, Operator hydrodynamics, otocs, and entanglement growth in systems without conservation laws, *Phys. Rev. X* **8**, 021013 (2018).
- [32] K. Klobas, B. Bertini, and L. Piroli, Exact thermalization dynamics in the “Rule 54” quantum cellular automaton, *Phys. Rev. Lett.* **126**, 160602 (2021).
- [33] K. Klobas and B. Bertini, Entanglement dynamics in Rule 54: Exact results and quasiparticle picture, *SciPost Phys.* **11**, 107 (2021).
- [34] N. Schuch, M. M. Wolf, F. Verstraete, and J. I. Cirac, Entropy scaling and simulability by matrix product states, *Phys. Rev. Lett.* **100**, 030504 (2008).
- [35] N. Schuch, M. M. Wolf, K. G. H. Vollbrecht, and J. I. Cirac, On entropy growth and the hardness of simulating time evolution, *New Journal of Physics* **10**, 033032 (2008).
- [36] A. Perales and G. Vidal, Entanglement growth and simulation efficiency in one-dimensional quantum lattice systems, *Phys. Rev. A* **78**, 042337 (2008).
- [37] P. Hauke, F. M. Cucchietti, L. Tagliacozzo, I. Deutsch, and M. Lewenstein, Can one trust quantum simulators?, *Reports on Progress in Physics* **75**, 082401 (2012).
- [38] B. Bertini, K. Klobas, V. Alba, G. Lagnese, and P. Calabrese, [arXiv:2203.17264](https://arxiv.org/abs/2203.17264) (2022).
- [39] S. Ghoshal and A. Zamolodchikov, Boundary S-matrix and boundary state in two-dimensional integrable quantum field theory, *Int. J. Mod. Phys. A* **09**, 3841 (1994).
- [40] L. Piroli, B. Pozsgay, and E. Vernier, What is an integrable quench?, *Nucl. Phys. B* **925**, 362 (2017).
- [41] A. Nahum, S. Vijay, and J. Haah, Operator spreading in random unitary circuits, *Phys. Rev. X* **8**, 021014 (2018).
- [42] A. Chan, A. De Luca, and J. T. Chalker, Solution of a minimal model for many-body quantum chaos, *Phys. Rev. X* **8**, 041019 (2018).
- [43] V. Khemani, A. Vishwanath, and D. A. Huse, Operator spreading and the emergence of dissipative hydrodynamics under unitary evolution with conservation laws, *Phys. Rev. X* **8**, 031057 (2018).
- [44] T. Rakovszky, F. Pollmann, and C. W. von Keyserlingk, Diffusive hydrodynamics of out-of-time-ordered correlators with charge conservation, *Phys. Rev. X* **8**, 031058 (2018).
- [45] B. Bertini, P. Kos, and T. Prosen, Exact spectral form factor in a minimal model of many-body quantum chaos, *Phys. Rev. Lett.* **121**, 264101 (2018).
- [46] A. J. Friedman, A. Chan, A. De Luca, and J. T. Chalker, Spectral statistics and many-body quantum chaos with conserved charge, *Phys. Rev. Lett.* **123**, 210603 (2019).
- [47] A. Chan, A. De Luca, and J. T. Chalker, Spectral statistics in spatially extended chaotic quantum many-body systems, *Phys. Rev. Lett.* **121**, 060601 (2018).
- [48] A. Flack, B. Bertini, and T. Prosen, Statistics of the spectral form factor in the self-dual kicked Ising model, *Phys. Rev. Research* **2**, 043403 (2020).
- [49] B. Bertini, P. Kos, and T. Prosen, Random matrix spectral form factor of dual-unitary quantum circuits, *Commun. Math. Phys.* **387**, 597 (2021).
- [50] F. Fritzsche and T. Prosen, Eigenstate thermalization in dual-unitary quantum circuits: Asymptotics of spectral functions, *Phys. Rev. E* **103**, 062133 (2021).
- [51] P. Kos, T. Prosen, and B. Bertini, Thermalization dynamics and spectral statistics of extended systems with thermalizing boundaries, *Phys. Rev. B* **104**, 214303 (2021).
- [52] B. Bertini, P. Kos, and T. Prosen, Exact spectral statistics in strongly localized circuits, *Phys. Rev. B* **105**, 165142 (2022).
- [53] S. J. Garratt and J. T. Chalker, Many-body delocalization as symmetry breaking, *Phys. Rev. Lett.* **127**, 026802 (2021).
- [54] S. J. Garratt and J. T. Chalker, Local pairing of Feynman histories in many-body Floquet models, *Phys. Rev. X* **11**, 021051 (2021).
- [55] A. Chan, S. Shivam, A. Huse, David, and A. De Luca, Many-body quantum chaos and space-time translational invariance, [arXiv:2109.04475](https://arxiv.org/abs/2109.04475) (2021).
- [56] K. Klobas and B. Bertini, Exact relaxation to Gibbs and non-equilibrium steady states in the quantum cellular automaton Rule 54, *SciPost Phys.* **11**, 106 (2021).
- [57] B. Bertini, P. Kos, and T. Prosen, Exact correlation functions for dual-unitary lattice models in 1 + 1 dimensions, *Phys. Rev. Lett.* **123**, 210601 (2019).
- [58] B. Bertini, P. Kos, and T. Prosen, Operator Entanglement in Local Quantum Circuits I: Chaotic Dual-Unitary Circuits, *SciPost Phys.* **8**, 67 (2020).

- [59] B. Bertini, P. Kos, and T. Prosen, Operator entanglement in local quantum circuits ii: Solitons in chains of qubits, *SciPost Physics* **8**, 68 (2020).
- [60] P. W. Claeys and A. Lamacraft, Maximum velocity quantum circuits, *Phys. Rev. Research* **2**, 033032 (2020).
- [61] I. Reid and B. Bertini, Entanglement barriers in dual-unitary circuits, *Phys. Rev. B* **104**, 014301 (2021).
- [62] P. W. Claeys and A. Lamacraft, Ergodic and non-ergodic dual-unitary quantum circuits with arbitrary local Hilbert space dimension, *Phys. Rev. Lett.* **126**, 100603 (2021).
- [63] R. Suzuki, K. Mitarai, and K. Fujii, Computational power of one- and two-dimensional dual-unitary quantum circuits, *Quantum* **6**, 631 (2022).
- [64] W. W. Ho and S. Choi, Exact emergent quantum state designs from quantum chaotic dynamics, *Phys. Rev. Lett.* **128**, 060601 (2022).
- [65] M. Ippoliti and W. W. Ho, [arXiv:2204.13657](https://arxiv.org/abs/2204.13657) (2022).
- [66] Y. Kasim and T. Prosen, [arXiv:2206.09665](https://arxiv.org/abs/2206.09665) (2022).
- [67] P. W. Claeys, M. Henry, J. Vicary, and A. Lamacraft, [arXiv:2207.00025](https://arxiv.org/abs/2207.00025) (2022).
- [68] C. Jonay, V. Khemani, and M. Ippoliti, Tri-unitary quantum circuits, [2106.07686](https://arxiv.org/abs/2106.07686) (2021).
- [69] R. Milbradt, L. Sheller, C. Assmus, and B. Mendl, Christian, Ternary unitary quantum lattice models and circuits in 2+1 dimensions, [arXiv:2206.01499](https://arxiv.org/abs/2206.01499) (2022).
- [70] P. W. Claeys and A. Lamacraft, Emergent quantum state designs and biunitarity in dual-unitary circuit dynamics, *Quantum* **6**, 738 (2022).
- [71] T. Zhou and A. W. Harrow, Maximal entanglement velocity implies dual unitarity, [arXiv:2204.10341](https://arxiv.org/abs/2204.10341) (2022).
- [72] B. Gutkin, P. Braun, M. Akila, D. Waltner, and T. Guhr, Local correlations in dual-unitary kicked chains, [arXiv:2001.01298](https://arxiv.org/abs/2001.01298) (2020).
- [73] F. Huber, C. Eltschka, J. Siewert, and O. Gühne, Bounds on absolutely maximally entangled states from shadow inequalities, and the quantum MacWilliams identity, *J. Phys. A: Math. Theor.* **51**, 175301 (2018).
- [74] S. A. Rather, A. Burchardt, W. Bruzda, G. Rajchel-Mieldzióć, A. Lakshminarayan, and K. Życzkowski, Thirty-six entangled officers of euler: Quantum solution to a classically impossible problem, *Phys. Rev. Lett.* **128**, 080507 (2022).
- [75] T. Prosen, Many-body quantum chaos and dual-unitarity round-a-face, *Chaos* **31**, 093101 (2021).
- [76] M. Borsi and B. Pozsgay, Remarks on the construction and the ergodicity properties of dual unitary quantum circuits (with an appendix by roland bacher and denis serre), [arXiv:2201.07768](https://arxiv.org/abs/2201.07768) (2022).
- [77] G. Giudice, G. Giudici, M. Sonner, J. Thoenniss, A. Leroose, D. A. Abanin, and L. Piroli, Temporal entanglement, quasiparticles and the role of interactions, *Phys. Rev. Lett.* **128**, 220401 (2022).
- [78] S. A. Rather, S. Aravinda, and A. Lakshminarayan, Creating ensembles of dual unitary and maximally entangling quantum evolutions, *Phys. Rev. Lett.* **125**, 070501 (2020).
- [79] S. Aravinda, S. A. Rather, and A. Lakshminarayan, From dual-unitary to quantum bernoulli circuits: Role of the entangling power in constructing a quantum ergodic hierarchy, *Phys. Rev. Research* **3**, 043034 (2021).
- [80] A. Rather, Suhail, S. Aravinda, and A. Lakshminarayan, Construction and local equivalence of dual-unitary operators: from dynamical maps to quantum combinatorial designs, [arXiv:2205.08842](https://arxiv.org/abs/2205.08842) (2020).
- [81] P. Facchi, G. Florio, G. Parisi, and S. Pascazio, Maximally multipartite entangled states, *Phys. Rev. A* **77**, 060304 (2008).
- [82] D. Goyeneche and K. Życzkowski, Genuinely multipartite entangled states and orthogonal arrays, *Phys. Rev. A* **90**, 022316 (2014).
- [83] P. Hosur, X.-L. Qi, D. A. Roberts, and B. Yoshida, Chaos in quantum channels, *Journal of High Energy Physics* **2016**, 1 (2016).
- [84] B. Bertini and L. Piroli, Scrambling in random unitary circuits: Exact results, *Phys. Rev. B* **102**, 064305 (2020).
- [85] T. Tao, *An Introduction to Measure Theory*, Graduate studies in mathematics (American Mathematical Society, 2013).
- [86] M. Ippoliti and V. Khemani, Postselection-free entanglement dynamics via spacetime duality, *Phys. Rev. Lett.* **126**, 060501 (2021).
- [87] F. Arute, K. Arya, R. Babbush, D. Bacon, J. C. Bardin, R. Barends, R. Biswas, S. Boixo, F. G. Brandao, D. A. Buell, *et al.*, Quantum supremacy using a programmable superconducting processor, *Nature* **574**, 505 (2019).
- [88] P. Kos and G. Styliaris, Circuits of space-time quantum channels, [arXiv:2206.12155](https://arxiv.org/abs/2206.12155) (2022).
- [89] A. Leroose, M. Sonner, and D. A. Abanin, Influence matrix approach to many-body Floquet dynamics, *Phys. Rev. X* **11**, 021040 (2021).
- [90] A. Leroose, M. Sonner, and D. A. Abanin, Scaling of temporal entanglement in proximity to integrability, *Phys. Rev. B* **104**, 035137 (2021).
- [91] M. Sonner, A. Leroose, and D. A. Abanin, Influence functional of many-body systems: Temporal entanglement and matrix-product state representation, *Ann. Physics* **435**, 168677 (2021).
- [92] M. Sonner, A. Leroose, and D. A. Abanin, Characterizing many-body localization via exact disorder-averaged quantum noise, *Phys. Rev. B* **105**, L020203 (2022).
- [93] A. Foligno, T. Zhou, and B. Bertini, Temporal entanglement in chaotic quantum circuits, in preparation (2022).